Field-dependent Abundances of Hydride Molecular Ions in Atom Probe Tomography of III-N Semiconductors

Aissatou Diagne[1], Louis Gonzalez Garcia[1], Samba Ndiaye[1], Noëlle Gogneau[2], Maria Vrellou[3], Jonathan Houard[1], Lorenzo Rigutti[1*]

[1] Univ Rouen Normandie, INSA Rouen Normandie, CNRS, Groupe de Physique des Matériaux UMR 6634, F-76000 Rouen, France

[2] Centre de Nanosciences et de Nanotechnologies, CNRS UMR 9001, Univ. Paris-Sud, Université Paris-Saclay, C2N – Orsay, 91405 Orsay Cedex, France

[3]Institute for Applied Materials, Karlsruhe Institute of Technology, Hermann von Helmholtz Platz 1, 76344 Eggenstein-Leopoldshafen, Germany

*Corresponding author, lorenzo.rigutti@univ-rouen.fr

Abstract

We investigate the microscopic behaviour of hydrogen-containing species formed on the surface of III-N semiconductor samples by the residual hydrogen in the analysis chamber in laser-assisted atom probe tomography (APT). We analysed AlGaN/GaN heterostructures containing alternate layers with a thickness of about 20 nm. The formation of H-containing species occurs at field strengths between 22 and 26 V/nm and is independent of the analysed samples. The 3D APT reconstruction makes it possible to map the evolution of the surface behaviour of these species issued by chemical reactions. The results highlight the strong dependence of the relative abundances of hydrides on the surface field during evaporation. The relative abundances of the hydrides decrease when the surface field increases due to the evolution of the tip shape or the different evaporation behaviour of the different layers.

1. Introduction

In the last two decades, laser-assisted Atom Probe Tomography (APT) has proved to be an efficient technique for mapping chemical species in semiconductors. Among its main achievements in microscopy of semiconductors, one could cite the elucidation of the alloy and doping distribution in III-N materials [1–5], the quantitative definition of interfaces in heterostructures [6], or the assessment of impurity segregation at defects [7,8]. However, it should not be forgotten that, despite the information of APT is visualised and analysed in a 3D virtual space, this technique is based on the surface phenomenon of field evaporation. Strictly speaking, APT should be considered as a surface microscopy technique, whose information is eventually summed up into a 3D system. Surface phenomena play an important role in APT compositional and spatial metrology, as they may have important consequences on the accuracy of the reconstructed images [9–14]. Among surface phenomena, one could cite the ionization of parasitic species contained in the chamber of analysis or even the reaction of surface atoms with them. Among parasitic species, hydrogen and oxygen are the most significant. In particular, hydrogen represents per se a domain of research in APT-based microscopy. Increasing attention is paid to it due to its importance as an energy vector [15]. Beyond that, it plays an important role in the determination of structural properties in metals [16–18], its interaction with functional defects in semiconductor bulk and surfaces [19,20]. Currently, several strategies are adopted in order to reduce the impact of parasitic H_2 within the analysis chamber. Its impact can be eliminated or reduced, for instance, by accurate choice of the materials and coating of the analysis chamber [21], or by deuterium charging of specimens [17,18,22]. However, the interaction of parasitic hydrogen with the specimen surface under high electric field can also be studied as an independent phenomenon. In a previous study, some of the authors of this article targeted the abundances of the hydrogen molecules H^+; H^{2+}, H_3^+

and their dependence on the electric field [23]. In this work, we study the formation of molecular ions containing both constituent atoms of semiconductor systems and hydrogen atoms from the surrounding environment. These problems are not only interesting for APT metrology, but may also be related to catalysis at the nanoscale [24]. The studied systems are AlGaN/GaN heterostructures containing alternating layers with nominally identical composition. This configuration is very useful for APT metrology studies as it allows inducing local changes in the surface field due to the fact that AlGaN is harder to evaporate than GaN. These field variations occur both in the radial and in the axial direction, due to a combination of feedback of the DC voltage applied to the tip and compositional variation during APT analysis at constant detection rate [14]. In fact, on an AlGaN layer the surface field required to sustain a given evaporation flux (and, for constant apex radius, a given detection rate) is higher than on a GaN layer [14]. The surface field within the analysed system varies between 22 and 26 V/nm. In this study, the charge state ratio (CSR) of the metallic element Me^{2+} /Me^{+} was used to estimate the electric field at the sample surface. This method is based on Kingham's theory of post-ionisation, according to which an ion may lose one or more electrons during the initial phases of the ion's acceleration in the field, so that higher charge states become statistically more frequent as the field increases [25].

This heterostructure configuration makes it possible to study the interactions between hydrogen and material on domains yielding local variations of the surface field. In fact, the main result of this work is highlighting the existence of several families of H-containing molecular ions, and that their abundances exhibit a strong dependence on the surface field.

2. Experimental details

A set of III-N semiconductor heterostructures was analysed in this study. The sample shown in the Figure 1a was fabricated by molecular beam epitaxy (MBE); the growth direction being

along the c polar axis. It contains superlattices with 20 periods of 20 nm layers of $Al_xGa_{1-x}N$/GaN with a nominal III-site fraction of Al $x \sim 0.7$ in the $Al_xGa_{1-x}N$ layers. Three different samples containing a different x Al III-site fraction in the AlGaN layers were analysed, yielding qualitatively similar results. In all samples, this alternation of layers was purposely designed for APT metrology experiments in order to monitor the variation in composition measured in samples containing upper and lower field layers for better accuracy in measurements.

Atom probe tip samples were obtained by standard lift-off and annular milling procedures based on focused ion beam (FIB) [26]. The analysis was carried out using a Laser-Assisted Wide-Angle Tomographic Atom Probe (LAWATAP). Laser pulses were generated using monochromatic UV light with a wavelength of 340 nm at a laser repetition frequency of 100 kHz. The detection system was a multichannel plate/advanced delay line detector (MCP/aDLD) with an MCP efficiency $\eta_{MCP} \approx 0.6$ [27] [28]. The temperature throughout the measurements was set at 50K. Although this parameter may have a significant impact on the analysis results, its investigation falls outside of our current scope.

Throughout the analysis, the laser energy remained constant. As the ions evaporate, the radius of the tip's curvature, progressively increases and consequently the amplitude of the electrostatic field decreases as well as the evaporation flux. To counterbalance this effect these two phenomena, the voltage V_{DC} applied to the tip was gradually modulated.

The pressure in the analysis chamber was of the order of 5×10^{-11} mbar, while the detection rate remained constant during the detection of over twenty million evaporated ions.

3. Results and Discussion

3.1 APT analysis: mass spectra

The mass spectrum obtained from this analysis is shown in the Figure 1b. The main species identified as material constituents are Al^{3+}, Al^{2+}, Al^{+} at 9, 13.5 and 27 Da respectively, the two isotope peaks of Ga^{+} (69 and 71 Da) and Ga^{2+} (34.5 and 35.5 Da), N^{+}, N^{2+} and N_2^{+} at 8, 14 (which may also be N_2^{2+}), and 28 Da respectively. Molecular species such as AlN^{2+} were identified at 20.5 Da.

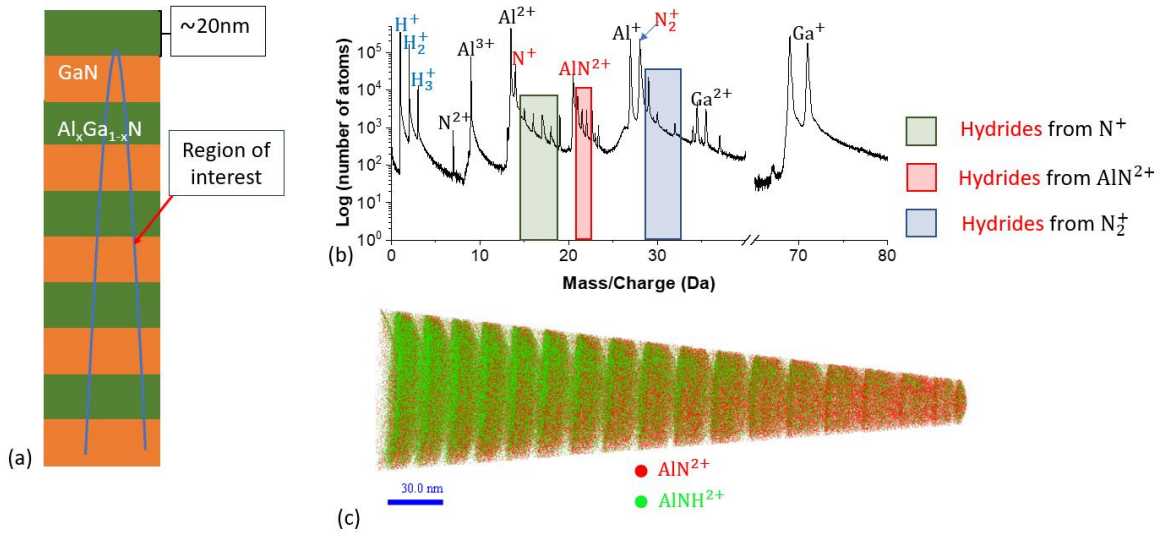

Figure 1: *(a) Schematic structure of the analyzed system (in blue, the approximate position of the APT specimen). (b) Mass spectrum from APT analysis of the AlGaN/GaN heterostructure. (c) 3D reconstructed volumes showing the spatial distribution of AlN^{2+} and $AlNH^{2+}$ molecular ion species.*

Parasitic species such as hydrogen ions H^{+}, H_2^{+} and H_3^{+} were identified at 1, 2 and 3 Da as seen in previous studies by Rigutti et al. [23]. These ions can be either hydrogen contained in the material or residual hydrogen present in the APT analysis chamber. Hydrides formed by matrix species were also identified as shown in Table 1. These hydrides could be formed by hydrogen in the analysis chamber during a reaction at the surface of the sample between the hydrogen and the elements of the matrix.

Main species (mass/charge in Da)	Hydrides (mass/charge in Da)			
$\mathbf{N^+}$ (14)	NH^+ (15)	NH_2^+ (16)	NH_3^+ (17)	NH_4^+ (18)
$\mathbf{N_2^+}$ (28)	N_2H^+ (29)	$N_2H_2^+$ (30)		$N_2H_4^+$ (32)
$\mathbf{AlN^{2+}}$ (20,5)	$AlNH^{2+}$ (21)	$AlNH_2^{2+}$ (21,5)	$AlNH_3^{2+}$ (22)	

Table 1: Main elements of the matrix and their relative hydrides with their respective mass-to-charge state ratio (in Da) allowing their identification on the mass spectrum.

Hydrogen is not the only parasitic species present in the material or in the analysis chamber. Oxygen may also be present due to residual gas in spite of the ultra-high vacuum in the analysis chamber. Thus, the peaks at 16, 17, 18 and 32 Da associated with the hydrides NH_2^+, NH_3^+, NH_4^+ and $N_2H_4^+$ respectively could also be identified as O^+, OH^+, H_2O^+ and O^{2+} respectively. However, in the rest of this study, all these peaks are assumed to be hydrides because we're not doing a composition calculation but looking at the dependence of these peaks on the surface field. Another important thing noticed during this analysis is the absence of a peak corresponding to the $N_2H_3^+$ species [29]. The fraction of nitrogen hydrides in the mass spectrum represents around 4.3% of the species identified.

A typical 3D reconstruction of an APT analysis highlighting the spatial distribution of AlN^{2+} and $AlNH^{2+}$ is shown in Figure 1c. This reconstruction is obtained by applying the "cone angle" algorithm with an initial radius R_0 = 25nm, curvature factor 1, compression factor M+1 = 1.6, cone angle 10° and reconstruction detection efficiency η_{rec}=0.25. Notice that this parameter is lower than the detector efficiency (η_{MCP} ~0.6) due to mechanisms of detection loss related to the evaporation of neutral ions and to preferential evaporation [3,14]. These geometric parameters are those given by default by the software used to process the data.

3.2 Field Estimation at the surface of the sample

The charge state ratio (CSR) for the species X is defined as

$$CSR(\mathrm{X}) = \frac{n(\mathrm{X}^{++})}{n(\mathrm{X}^{+})},$$

where n(X) is the number of ions of species X detected within a given spatial interval. The main advantage of the CSR(Ga) is that it may be exploited as a microscopic field indicator in all layers. The correlation between the CSR and the local field is shown in the figure 2a as directly issued by the Kingham model [30]. Considering the CSR(Ga) we can see that the higher this ratio is, the more intense the field becomes. This quantity can be calculated locally by arbitrarily choosing a volume in the 3D reconstruction. This mapping of the local electric field can be correlated with the relative abundances of the hydrides to determine their behaviour at the surface of the material. The Figure 2b shows the 2D maps of the sample obtained from a 5-nm thick cross-section along the main axis (Z coordinate) of the tip. It maps the Al sites fraction to the left and the CSR(Ga) to the right. It is important to mention that the compositional gradient appearing in this representation are mostly an artefact, as they derive from intrinsic bias affecting both the spatial precision and the compositional accuracy of the analysis of AlGaN. These effects, also visible in the Figure 1c, have been studied in depth elsewhere [3,14] and are out of the scope of this work.

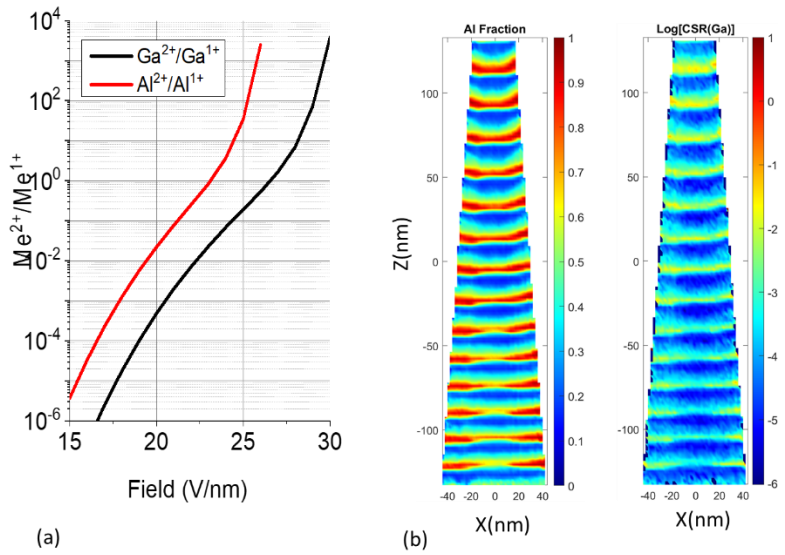

Figure 2: (a) Calculated correlation diagram between the CSR of Al and Ga and the local field. (b) Cross-sectional map of 5-nm thick along Z axis extracted from the reconstructed volume of the analysed specimen (Al sites fraction); (c) Ga charge state ratio.

From this representation of the CSR, it is evident that the strength of the field varies depending on the periodic structure of the material ($Al_xGa_{1-x}N$/GaN). Specifically, the field is stronger on an $Al_xGa_{1-x}N$ layer compared to a GaN layer, due to the difference in the strength between the Al-N and Ga-N bonds. For the GaN layers, the field is also generally more intense close to the axis of the tip than far from it. For the $Al_xGa_{1-x}N$ layers there is an apparent decrease of the field towards the axis, which could be due to a partial intermixing of GaN and $Al_xGa_{1-x}N$ reconstructed layers. This reconstruction artefact lowers the interface resolution for the present experimental conditions, and has the secondary effect of increasing the scattering of the data presented in Figure 3b. If we look at the map as a whole, the field is stronger at the apex and this intensity decreases along the tip. This decrease of the field is due to the increase of the imaged surface within the detector field of view. As the detection rate, which is kept constant, is the product of the evaporation rate and of the imaged surface, the field decreases to keep the

detection rate constant [31]. This estimate of the local field makes it possible to study the formation of hydride species on the surface of the material.

3.3 Dependence of hydrides formation on the surface electric field

In the remainder of this work, the quantity used to study the behaviour of the hydrides at the surface of the sample and to correlate it with the electric field, is the relative abundance. This quantity is calculated for each family of species using the total number of ions detected for each species identified. It is defined as follows for the family of N_2^+ and its hydrides N_2H^+, $N_2H_2^+$ and $N_2H_4^+$ for example:

$$A(N_2H_i^+) = \frac{n(N_2H_i^+)}{n(N_2^+) + n(N_2H^+) + n(N_2H_2^+) + n(N_2H_4^+)}$$

Where i = 0, 1, 2 and 4 is the number of hydrogen atoms in the molecule, n is the total number of ions evaporated contained in the interval defined on the mass spectrum of each species identified.

The field estimate shows that the field is stronger on an AlGaN layer than on a GaN layer. Several parameters can influence the evolution of the field at the surface of the material: the structure of the sample, the crystallographic orientation and the area imaged, which increases during the analysis with a constant detection rate [32]. The 2D maps shown in the figure 3a were obtained using the same process described in section **3.2** for mapping the CSR(Ga) and Al sites fraction. They show from left to right the charge state ratio of Ga (repeated here for clarity) and the relative abundances of N_2^+species and its relative hydrides (N_2H^+, $N_2H_2^+$, and $N_2H_4^+$) respectively.

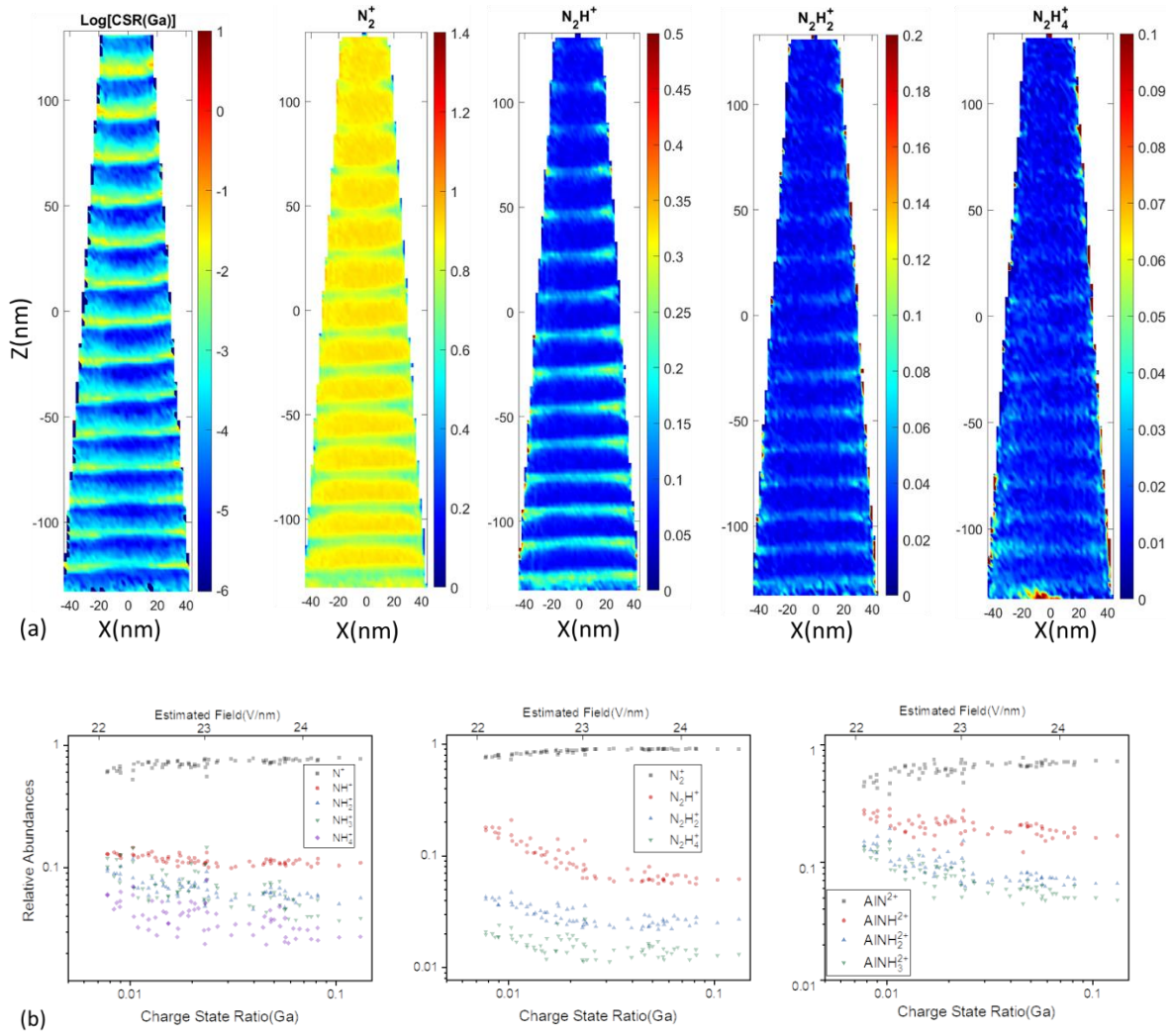

Figure 3: (a) Cross-sectional map extracted from the reconstructed volume of the analysed specimen of Ga charge states ration at left, and the relative abundances of the N_2^+ family and its relative hydrides N_2H^+, $N_2H_2^+$ and $N_2H_4^+$. (b) Correlation diagrams representing, from left to right, the relative abundances of the N^+, N_2^+ and AlN^{2+} families and their relative hydrides respectively.

It can be seen from these representations that the variation of the hydrides follows the evolution of the surface field. In layers where the field is stronger (AlGaN layers), fewer hydrides are formed, and in layers where the field is weaker (GaN layers), more hydrides are formed. To illustrate this dependence of hydride formation on the surface field, the correlation diagrams between the field and the relative abundances of the three families of hydrides identified on the

mass spectrum are shown in the figure 3b. From left to right we have the families N^+ and relative hydrides, N_2^+ and its hydrides, AlN^{2+} and its hydrides respectively. What is important to note here is that the hydrides in the three families all show similar trends. Their relative abundances decrease as the electric field increases [33]. The trend is less pronounced in the case of the NH_n^+ species. The main conclusion to draw from these results is that hydrides form preferentially at low fields, and that this formation is independent of the relative fraction of elements of group III in the nitride. The exact mechanism of formation of molecular ions from parasitic gases are not elucidated yet, although this is quite consistent with a general trend stating that the formation of molecular ions (either containing parasitic gases or only constituent atoms) prevails at lower field and/or high laser energy in laser-assisted APT [34,35]. This may be due either to a different dynamics of surface interaction or to the increased probability of dissociation of molecular ions in a higher electric field [12,36,37]. In order to obtain a deeper insight into this problem, a thorough analysis of multiple detection events has to be implemented in a future work, but correlation with numerical calculations would also improve the interpretation.

4. Conclusions and Outlook

In conclusion, the microscopic behaviour of nitrogen hydrides at the surface of AlGaN/GaN semiconductor heterostructures was studied. For all the families of hydrides identified, the evolution of their relative abundances follows the same trends as a function of the field, the estimation of which gives us a range of variation of 22-26 V/nm. This shows that the relative abundances of hydrides depend on the electric field, and are independent of the fraction of element III present in the nitride phase. This result represents a first step in the understanding

of the chemical reactions that take place at the surface of the material, leading to the formation of hydride molecular ions.

In perspective, the study of multiple-ion events (i.e. when several ions are detected on the same pulse) between matrix compounds and hydrogen would be important to gain insight into hydride formation, along with an investigation of the chemical reactions that can take place at the material surface. Other parameters that could influence hydride formation during evaporation, such as temperature applied to the sample, laser energy, partial pressure of hydrogen in the analysis chamber, etc., are also of interest. A particular interest would be represented by studies on systems that have a high affinity with H, such as Zirconium, Titanium and Magnesium-based materials [38], in order to elucidate the interactions between hydrogen and the constituent atoms of these materials, which may also be used for hydrogen storage.

Acknowledgements

This work has been funded by the French National Research Agency (ANR) in the framework of the LABEX EMC3 “Quantiphy” project.

References

[1] Galtrey, M.J. et al. (2007). Three-dimensional atom probe studies of an InxGa1−xN⁄GaN multiple quantum well structure: Assessment of possible indium clustering. *Applied Physics Letters*. DOI: 10.1063/1.2431573.

[2] Bennett, S.E. et al. (2011). Atom probe tomography and transmission electron microscopy of a Mg-doped AlGaN/GaN superlattice. *Ultramicroscopy*. DOI: 10.1016/j.ultramic.2010.11.028.

[3] Rigutti, L. et al. (2016). Statistical correction of atom probe tomography data of semiconductor alloys combined with optical spectroscopy: The case of Al0.25Ga0.75N. *Journal of Applied Physics*. DOI: 10.1063/1.4943612.

[4] Licata, O.G. et al. (2021). Dopant-defect interactions in Mg-doped GaN via atom probe tomography. *Applied Physics Letters*. DOI: 10.1063/5.0061153.

[5] Amichi, L. et al. (2019). Correlative investigation of Mg doping in GaN layers grown at different temperatures by atom probe tomography and off-axis electron holography. *Nanotechnology*. DOI: 10.1088/1361-6528/ab4a46.

[6] Mazumder, B. et al. (2013). Atom probe analysis of AlN interlayers in AlGaN/AlN/GaN heterostructures. *Applied Physics Letters*. DOI: 10.1063/1.4798249.

[7] Thompson, K. et al. (2007). Imaging of Arsenic Cottrell Atmospheres Around Silicon Defects by Three-Dimensional Atom Probe Tomography. *Science*. DOI: 10.1126/science.1145428.
[8] Mancini, L. et al. (2016). Multi-microscopy study of the influence of stacking faults and three-dimensional In distribution on the optical properties of m-plane InGaN quantum wells grown on microwire sidewalls. *Applied Physics Letters*. DOI: 10.1063/1.4940748.
[9] Gault, B. (2009). Advances in the calibration of atom probe tomographic reconstruction. *Journal of Applied Physics*. DOI: 10.1063/1.3068197.
[10] Vurpillot, F. et al. (2016). Accuracy of analyses of microelectronics nanostructures in atom probe tomography. *Semiconductor Science and Technology*. DOI: 10.1088/0268-1242/31/7/074002.
[11] Gault, B. et al. (2010). Influence of surface migration on the spatial resolution of pulsed laser atom probe tomography. *Journal of Applied Physics*. DOI: 10.1063/1.3462399.
[12] Gault, B. et al. (2016). Behavior of molecules and molecular ions near a field emitter. *New Journal of Physics*. DOI: 10.1088/1367-2630/18/3/033031.
[13] Mancini, L. et al. (2014). Composition of Wide Bandgap Semiconductor Materials and Nanostructures Measured by Atom Probe Tomography and Its Dependence on the Surface Electric Field. *The Journal of Physical Chemistry C*. DOI: 10.1021/jp5071264.
[14] Di Russo, E. et al. (2018). Composition Metrology of Ternary Semiconductor Alloys Analyzed by Atom Probe Tomography. *The Journal of Physical Chemistry C*. DOI: 10.1021/acs.jpcc.8b03223.
[15] Turner, J.A. (2004). Sustainable Hydrogen Production. *Science*. DOI: 10.1126/science.1103197.
[16] Daw, M.S. et Baskes, M.I. (1983). Semiempirical, Quantum Mechanical Calculation of Hydrogen Embrittlement in Metals. *Physical Review Letters*. DOI: 10.1103/PhysRevLett.50.1285.
[17] Takahashi, J. et al. (2012). Direct observation of hydrogen-trapping sites in vanadium carbide precipitation steel by atom probe tomography. *Scripta Materialia*. DOI: 10.1016/j.scriptamat.2012.04.022.
[18] Chen, Y.-S. et al. (2017). Direct observation of individual hydrogen atoms at trapping sites in a ferritic steel. *Science*. DOI: 10.1126/science.aal2418.
[19] Stavola, M. et al. (1988). Hydrogen Motion in Defect Complexes: Reorientation Kinetics of the B-H Complex in Silicon. *Physical Review Letters*. DOI: 10.1103/PhysRevLett.61.2786.
[20] Van de Walle, C.G. et Neugebauer, J. (2006). Hydrogen in Semiconductors. *Annual Review of Materials Research*. DOI: 10.1146/annurev.matsci.36.010705.155428.
[21] Felfer, P.J. (2019). A Toolchain for the Analysis of Hydrogen in Materials at the Atomic Scale. *Microscopy and Microanalysis*. DOI: 10.1017/S1431927619002125.
[22] Chang, Y.H. et al. (2019). Quantification of solute deuterium in titanium deuteride by atom probe tomography with both laser pulsing and high-voltage pulsing: influence of the surface electric field. *New Journal of Physics*. DOI: 10.1088/1367-2630/ab1c3b.
[23] Rigutti, L. et al. (2021). Surface Microscopy of Atomic and Molecular Hydrogen from Field-Evaporating Semiconductors. *The Journal of Physical Chemistry C*. DOI: 10.1021/acs.jpcc.1c04778.
[24] Dubau, L. et al. (2015). Tuning the Performance and the Stability of Porous Hollow PtNi/C Nanostructures for the Oxygen Reduction Reaction. *ACS Catalysis*. DOI: 10.1021/acscatal.5b01248.
[25] David R. Kingham (1982). THE POST-IONIZATION OF FIELD EVAPORATED IONS: A THEORETICAL EXPLANATION OF MULTIPLE CHARGE STATES. *Surf. Sci.*
[26] Blum, I. et al. (2016). Atom Probe Sample Preparation, in *Atom Probe Tomography*, Elsevier, p. 97-121.
[27] Da Costa, G. et al. (2005). Design of a delay-line position-sensitive detector with improved performance. *Review of Scientific Instruments*. DOI: 10.1063/1.1829975.
[28] Costa, G.D. et al. (2012). Advance in multi-hit detection and quantization in atom probe tomography. *Review of Scientific Instruments*. DOI: 10.1063/1.4770120.

[29] Matus, M.H. et al. (2006). The Heats of Formation of Diazene, Hydrazine, $N_2H_3^+$, $N_2H_5^+$, N_2H, and N_2H_3 and the Methyl Derivatives CH_3NNH, CH_3NNCH_3, and $CH_3HNNHCH_3$. *The Journal of Physical Chemistry A*. DOI: 10.1021/jp061854u.
[30] Kingham, D.R. (1982). The post-ionization of field evaporated ions: A theoretical explanation of multiple charge states. *Surface Science*. DOI: 10.1016/0039-6028(82)90434-4.
[31] Ndiaye, S. et al. (2023). Surface Dynamics of Field Evaporation in Silicon Carbide. *The Journal of Physical Chemistry C*. DOI: 10.1021/acs.jpcc.2c08908.
[32] Rigutti, L. et al. (2021). Surface Microscopy of Atomic and Molecular Hydrogen from Field-Evaporating Semiconductors. *The Journal of Physical Chemistry C*. DOI: 10.1021/acs.jpcc.1c04778.
[33] Tsong, T.T. FIELD PROMOTED AND SURFACE CATALYZED FORMATION OF H, AND NH, ON TRANSITION METAL SURFACES: A PULSED-LASER IMAGING ATOM-PROBE STUDY.
[34] Kellogg, G.L. et Tsong, T.T. (1980). Pulsed-laser atom-probe field-ion microscopy. *Journal of Applied Physics*. DOI: 10.1063/1.327686.
[35] Thuvander, M. et al. (2011). Quantitative atom probe analysis of carbides. *Ultramicroscopy*. DOI: 10.1016/j.ultramic.2010.12.024.
[36] Zanuttini, D. et al. (2017). Simulation of field-induced molecular dissociation in atom-probe tomography: Identification of a neutral emission channel. *Physical Review A*. DOI: 10.1103/PhysRevA.95.061401.
[37] Hans, M. et Schneider, J.M. (2020). Electric field strength-dependent accuracy of TiAlN thin film composition measurements by laser-assisted atom probe tomography. *New Journal of Physics*. DOI: 10.1088/1367-2630/ab7770.
[38] Mouton, I. et al. (2019). Quantification Challenges for Atom Probe Tomography of Hydrogen and Deuterium in Zircaloy-4. *Microscopy and Microanalysis*. DOI: 10.1017/S143192761801615X.